Biomaterials 172 (2018) 30–40

Contents lists available at ScienceDirect

Biomaterials

journal homepage: www.elsevier.com/locate/biomaterials

# Microdevice arrays with strain sensors for 3D mechanical stimulation and monitoring of engineered tissues

Haijiao Liu [a, b, c], Luke A. MacQueen [a], Jenna F. Usprech [b, c], Hoda Maleki [a, c], Krista L. Sider [a], Matthew G. Doyle [a], Yu Sun [a, b, **], Craig A. Simmons [a, b, c, *]

[a] Department of Mechanical and Industrial Engineering, University of Toronto, Toronto, M5S 3G8, Canada
[b] Institute of Biomaterials and Biomedical Engineering, University of Toronto, Toronto, M5S 3G9, Canada
[c] Translational Biology and Engineering Program, Ted Rogers Centre for Heart Research, Toronto, M5G 1M1, Canada

## ARTICLE INFO

*Article history:*
Received 4 February 2018
Received in revised form
18 April 2018
Accepted 21 April 2018
Available online 23 April 2018

*Keywords:*
Microdevice
Mechanical stimulation
On-chip strain sensing
Tissue stiffness monitoring
Hydrogel
Mesenchymal stromal cell

## ABSTRACT

Native and engineered tissue development are regulated by the integrative effects of multiple microenvironmental stimuli. Microfabricated bioreactor array platforms can efficiently dissect cue-response networks, and have recently integrated critical 2D and 3D mechanical stimulation for greater physiological relevance. However, a limitation of these approaches is that assessment of tissue functional properties is typically limited to end-point analyses. Here we report a new deformable membrane platform with integrated strain sensors that enables mechanical stretching or compression of 3D cell-hydrogel arrays and simultaneous measurement of hydrogel construct stiffness in situ. We tested the ability of the integrated strain sensors to measure the evolution of the stiffness of cell-hydrogel constructs for two cases. First, we demonstrated in situ stiffness monitoring of degradable poly (ethylene glycol)-norbornene (PEG-NB) hydrogels embedded with mesenchymal stromal cells (MSCs) and cultured with or without cyclic tensile stimulation for up to 15 days. Whereas statically-cultured hydrogels degraded and softened throughout the culture period, mechanically-stimulated gels initially softened and then recovered their stiffness corresponding to extensive cell network and collagen production. Second, we demonstrated in situ measurement of compressive stiffening of MSC-seeded PEG-NB gels cultured statically under osteogenic conditions, corresponding to increased mineralization and cellularization. This measurement technique can be generalized to other relevant bioreactor and organ-on-a-chip platforms to facilitate online, non-invasive, and high-throughput functional analysis, and to provide insights into the dynamics of engineered tissue development that are otherwise not available.

## 1. Introduction

Tissue development, homeostasis and disease are influenced by the integration of multiple environmental cues, including biochemical stimuli, mechanical forces, and extracellular matrix material properties [1,2]. Cell-driven tissue responses to one type of stimulus can be modulated by other environmental cues, resulting in context-specific responses [3]. In vitro efforts to understand complex interactions between multiple microenvironmental stimuli have been limited by the low experimental throughput of traditional bioreactors. To address this need, microfabricated bioreactor arrays have been developed to combinatorially prescribe and probe multiple environmental stimuli to systematically define cue-response relationships [4–8]. For example, Figallo et al. developed a device with arrayed culture wells to enable systematic and precise variation of mass transport and hydrodynamic shear to study their effects on stem cell functions [6], and Gobaa et al. developed a platform with an array of soft hydrogel microwells that simultaneously probed substrate stiffness and combinations of adhesion proteins on stem cell fate [8].

Bioreactor array platforms have provided important insights into the regulatory roles of specific environmental stimuli and their interactions on cell fate and tissue development [9–11]. However, despite the critical regulating effects of 3D mechanical stimulation on cell and tissue function [12–14], there are few examples of

---

* Corresponding author. Department of Mechanical and Industrial Engineering, University of Toronto, Toronto, M5S 3G8, Canada.

** Corresponding author. Department of Mechanical and Industrial Engineering, University of Toronto, Toronto, M5S 3G8, Canada.

*E-mail addresses:* sun@mie.utoronto.ca (Y. Sun), simmons@mie.utoronto.ca (C.A. Simmons).

https://doi.org/10.1016/j.biomaterials.2018.04.041

bioreactor array platforms that include mechanical stimuli. To address this need, we and others have developed microfabricated platforms that apply 2D dynamic mechanical stretch to cells adhered to deformable membrane arrays [15,16]. These platforms have been used to study the mechanobiological responses of cells to combinations of matrix proteins, growth factors, and 2D dynamic stretch, with higher throughput than standard cell stretching systems [15]. Performing similar systematic, combinatorial experiments in 3D mechanically active environments is also of broad interest, particularly for tissue engineering applications in which microenvironmental stimuli can be used to guide cell function and tissue formation in vitro [5,17–19]. For some tissues, such as cartilage and intervertebral disc [20,21], tissue growth is predominantly modulated by compressive forces, whereas other tissues such as heart muscle, heart valves, blood vessels and bladder benefit from 3D loading that includes in-plane tension for tissue growth [22,23]. Thus, we have adapted our deformable membrane platforms to enable both 3D mechanical compression [24,25] and stretching [26] of arrays of cell-seeded hydrogel constructs, which enable combinatorial investigation of a variety of relevant mechanobiological stimuli on cell fate and function and optimization of culture conditions.

A limitation of these approaches, and indeed most bioreactor-based approaches for tissue engineering, is that assessment of tissue functional properties is limited to end-point analysis [27–29]. End-point analysis is inherently destructive and requires manual and offline assays with bulky analytical equipment. In contrast, continuous monitoring of the functional status of engineered tissues would provide information on dynamic changes in tissue development and enable feedback for appropriate control and optimization, akin to other bioprocesses. However, there are few examples of bioreactor array platforms [30] capable of quantitatively tracking the functional status of tissue development, with cellular analysis being the most common approach [6,31–33]. However, cellular markers are not necessarily reflective of tissue functions, particularly for load-bearing tissues in which tissue mechanical properties are among the gold standard function metrics.

To address this need, we report here a deformable membrane platform that enables mechanical stretching or compression of 3D cell-hydrogel arrays and simultaneously performs continuous stiffness measurement of the hydrogel constructs in situ with integrated strain sensors. We demonstrate that the integrated strain sensors are able to monitor hydrogel stiffness changes that correlate with matrix degradation, collagen synthesis, and mineralization. Our platform represents a promising approach to address the limitation of end-point analysis, enabling exploration of bioprocess control strategies and providing insights otherwise not available into the evolution of engineered tissues.

## 2. Materials and methods

### 2.1. Device fabrication

Building on our previous bulging membrane platforms [15,24,26], we have developed a new device array that applies dynamic 3D mechanical stimulation to soft biological tissues in the device and performs continuous on-chip tissue stiffness measurement (Fig. 1A). Specifically, we applied 3D mechanical stretching to the hydrogels by covalently bonding them to the bulging membranes, as shown in Fig. 1. Carbon nanotube (CNT)-based strain sensors, which exhibit strain-dependent electrical resistivity [24], were patterned and embedded in the deformable membranes to provide on-chip measurement of membrane deflection for estimating tissue stiffness. Membrane deflection is proportional to the sample tissue's stiffness, and thus the magnitude of sensor's resistive strain, $|\Delta R/R_0|$, vs. input pressure permitted the measurement of the samples' elastic moduli (Fig. 2).

To fabricate the bulging membrane platform with integrated strain sensors, off-stoichiometry thiol-ene based polydimethylsiloxane (OSTE-PDMS) was mixed at a composition ratio of 2:0.3:1.5:1.5:1.5 and poured onto an aluminum master mold. The mold contained features of pressure chambers and channel at a height of 0.25 mm. OSTE-PDMS was casted against the mold to a final height of 1 mm. OSTE-PDMS was cured with 365 nm UV light for two minutes at an average dose of 6.3 mW/cm$^2$, peeled off the aluminum mold and cut into strips having 3 × 8 membranes with each column connected by underlying single channels. These OSTE-PDMS strips were then bonded to glass substrates by first spin coating a ~10 μm-thick mortar layer of OSTE-PDMS on the glass, then placing the cured OSTE-PDMS device layer onto the coated glass slide and curing with UV for one minute. Then connection ports were punched with biopsy punches and connected to tubing.

Strain sensors were fabricated by screen printing strips of uncured CNT: OSTE-PDMS blends (mixed at 1:12 ratio in weight) over the OSTE-PDMS membranes and curing with UV for two minutes. The sensor strips typically had 50 μm thickness, 300 μm width and 1.4 cm length. One sensor strip was placed through the middle of each circular deformable membrane, which was of 5 mm diameter and spaced by 9 mm center to center from other deformable membranes. Electrical connectors were then bonded to the glass slide using cyanoacrylate super glue and connected to the strain sensor strips by applying additional uncured CNT: OSTE-PDMS blends, which were then cured with UV again for two minutes. The sensors and sensor-electrode interconnects were then passivated by spin coating ~100 μm-thick layer of OSTE-PDMS (Fig. 1C). Membrane deflection magnitude and strain sensor signals were calibrated against applied actuation pressure. Membrane bulging heights were experimentally measured using a telescopic lens (Fig. 1D). After calibration, the culture chamber pre-made of regular Sylgard PDMS was bonded to the device layer. Fig. 1B shows a completed device containing culture medium for applying 3D mechanical stretching.

### 2.2. Cell and tissue culture

Cryopreserved human bone marrow-derived MSCs were obtained from the Texas A&M Health Science Center College of Medicine Institute for Regenerative Medicine at Scott &White through a grant from NCRR of the NIH, Grant # P40RR017447. Passage 5 MSCs and complete culture medium containing 81.7% α-MEM with L-glutamine, 16.3% fetal bovine serum, 1% additional L-glutamine and 1% penicillin/streptomycin were used for all experiments. MSCs-seeded hydrogel constructs were cultured and mechanically stimulated with 5% nominal tensile strain at 0.1 Hz for 8 h/day for 15 days (Fig. S1). Culture medium supplemented with 100 μM ascorbic acid was changed every day. For static conditions, the gels were cultured without mechanical stimulation except during the measurement cycles, which were limited to 20–30 min duration applied every two to three days to minimize the effects of mechanical loading on cells. The cell-laden hydrogel arrays were cultured in 150 mm Petri dishes and maintained in a humidified 37 °C incubator with 5% $CO_2$.

### 2.3. PEG-NB hydrogel model system

OSTE-PDMS membranes were used to covalently bind poly (ethylene glycol)-norbornene (PEG-NB) hydrogels, a model biomaterial with tunable adhesion peptide identities and densities, elasticity, and degradability. PEG-NB was synthesized and

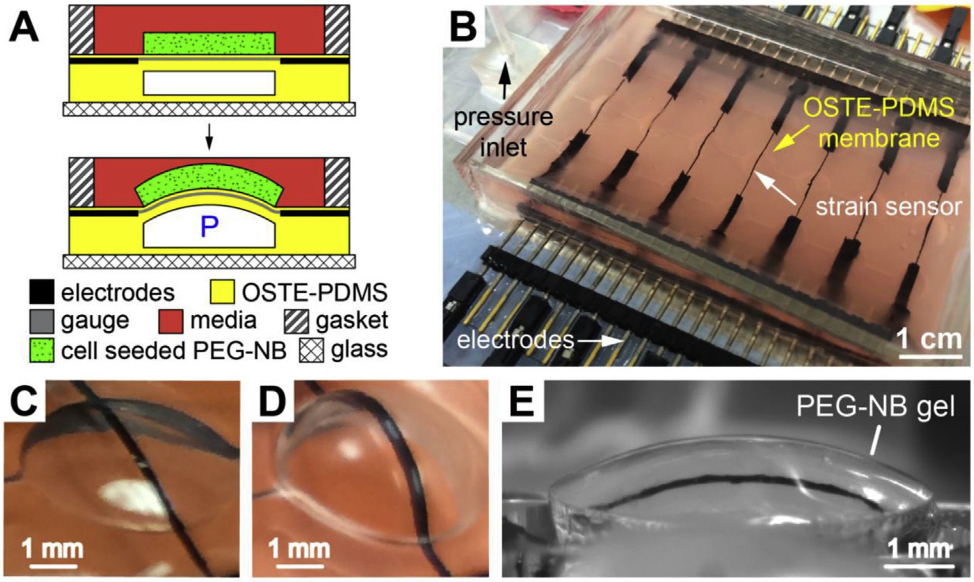

**Fig. 1.** Deformable membrane platform with integrated CNT strain sensors for simultaneous 3D mechanical stimulation and measurement of cell-seeded hydrogel construct arrays. (A) Cell-seeded PEG-NB hydrogels are bound to deformable membranes via a thiol-ene reaction with OSTE-PDMS as the membrane material. Bonding to OSTE-PDMS enabled the 3D hydrogel to be cyclically deformed and stretched by the membrane. Nanotube-based strain sensors provide continuous readout of membrane deflection magnitude; P = pressure. (B) Example of a microdevice with integrated CNT sensors. Electrode leads are embedded in OSTE-PDMS for electrical insulation. Example of a single deformable membrane unit with embedded CNT sensor at rest (C), being deformed without (D) and with the bound PEG-NB gel (E).

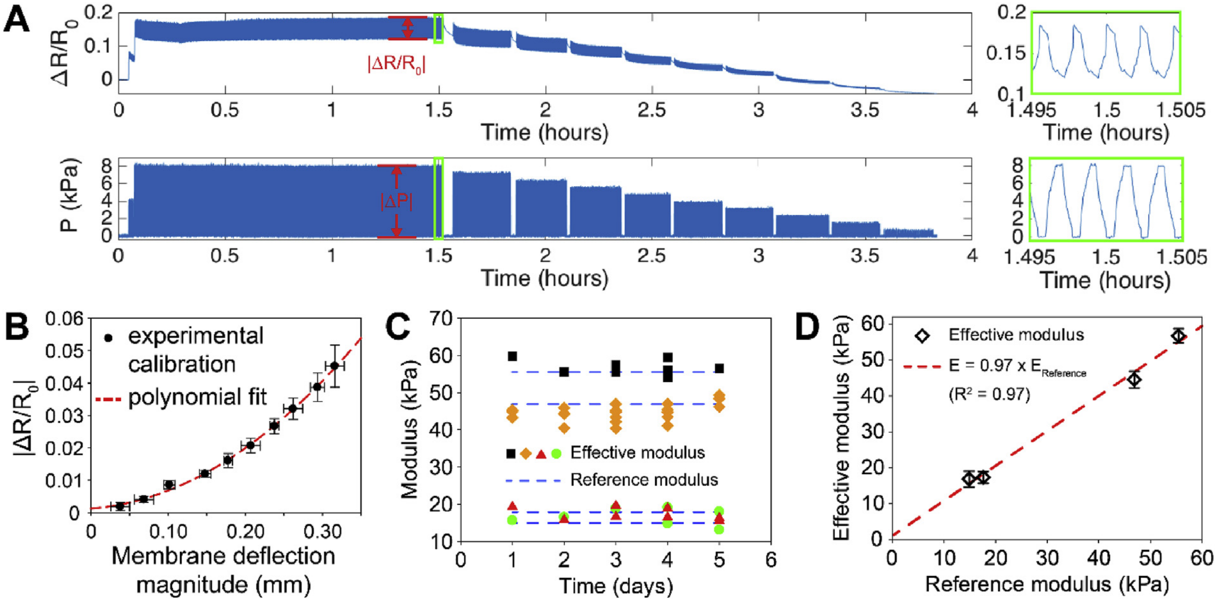

**Fig. 2.** Sensor calibration and measurement of elastic modulus of non-degradable PEG-NB gel. (A) Calibration signal of resistive strain, $\Delta R/R_0$ (top), corresponding to cyclic actuation pressure (bottom). Right: zoom-in of signals outlined in green; (B) Calibration curve of membrane deflection magnitude correlating with the resistive strain magnitude $|\Delta R/R_0|$. Number of sensors analyzed = 9, data are the mean ± SD, $R^2 = 0.998$; experimentally collected strain sensor signal was converted to membrane deflection, which was used as input via inverse finite element analysis to calculate the effective modulus of PEG-NB. (C) Effective moduli of non-degradable PEG-NB gels calculated from the sensor signal remained relatively constant over time, as expected. The reference moduli from standard mechanical compression testing were overlaid on top for comparison. Each type of marker represents a sample with a distinct stiffness. (D) Effective moduli estimated using our microdevice vs. those measured using the reference platform. The dashed line is a linear best fit of the data; data are the mean ± SD (n = 5). (For interpretation of the references to colour in this figure legend, the reader is referred to the Web version of this article.)

crosslinked to bond to OSTE-PDMS as previously described [26]. Lyophilized PEG-NB was dissolved in 10 mM phosphate buffered saline (1× PBS) to a final concentration of 6% w/v (3 mM) when combined with 0.05% w/v Irgacure 2959 photoinitiator (BASF) and 14.7 mM of 3.4 kDa PEG-dithiol crosslinker (PEG-DT, Laysan Bio) to achieve 50% of crosslinking density to form the non-degradable PEG-NB hydrogels, for validation experiments. The prepolymer solution of PEG-NB hydrogels was added onto a thin mortar layer of uncured OSTE-PDMS and irradiated with UV light for two minutes to polymerize the gel and bond it to OSTE-PDMS via the thiol-ene reaction (Fig. 1E).

To enhance cell adhesion and allow for cell-mediated matrix

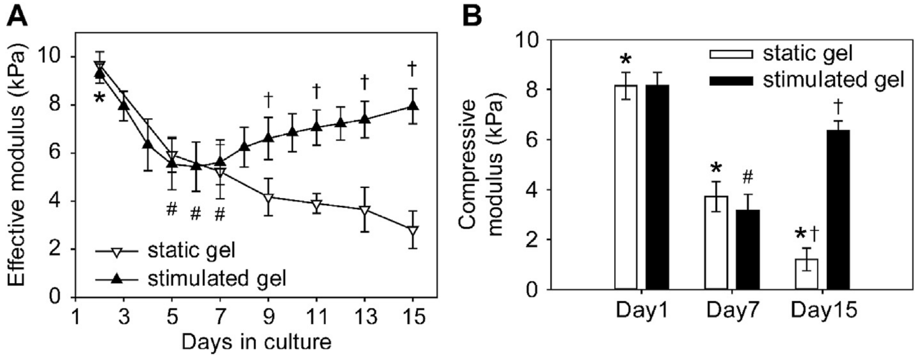

**Fig. 3.** (A) Time-dependent effective modulus of cell-embedded PEG-NB gels (*$p < 0.04$ vs. all other groups in static condition, #$p < 0.05$ vs. day 1 in stimulated condition, †$p < 0.05$ between static and stimulated conditions at each corresponding day, $n = 3$ per group). (B) Standard mechanical compression test of conditioned gels (*$p < 0.05$ and †$p < 0.001$ between groups with symbol, #$p < 0.005$ vs. other groups in stimulated condition, $n = 3–6$ per group). Error bars indicate s.e.m.

remodeling, the cell degradable PEG-NB was decorated with CRGDS adhesion peptides (GenScript) and crosslinked using the matrix metalloproteinase (MMP)-degradable peptide sequence KCGGPQGIWGQGCK, which is flanked with thiol-containing cysteine groups (GenScript). MSCs suspended in 1× PBS were mixed 1:3 with PEG-NB prepolymer solution, which contained a final concentration of 8% w/v of PEG-NB, 35% crosslinking density, 2.5 mM CRGDS, 0.05% w/v Irgacure 2959 photoinitiator and $1 \times 10^6$ cells/mL. No other PEG-NB concentrations or crosslinking densities were considered in this study; a previous study investigated MSC responses to different PEG-NB concentrations in static conditions [10].

To integrate the cell seeded PEG-NB hydrogels onto the OSTE-PDMS bulging membrane device, a mortar layer of uncured OSTE-PDMS was first applied on top of the device (Fig. 1A). Stencils of regular Sylgard PDMS, containing an array of cylindrical opening (6 mm diameter and 1 mm height), were sterilized and aligned on the mortar layer concentrically to the OSTE-PDMS membrane unit. Next, a transparency photomask with a 5 mm diameter opening window was assembled onto the PDMS stencil and aligned concentrically to the membrane below. 30 μL of the cell-laden PEG-NB prepolymer solution was added to each stencil well. The mixture of PEG-NB solution and cells, together with the OSTE-PDMS mortar layer were cured under UV light for two minutes. The uncured mixture of PEG-NB and cells were washed away with PBS. Finally, the photomask and PDMS stencils were sequentially peeled off, leaving the cell seeded PEG-NB hydrogels covalently bound to the OSTE-PDMS membrane.

### 2.4. Device operation and strain sensor calibration

A diaphragm pump (Shwarzer, model SP 500EC) and a programmable pressure regulator (Marsh Bellofram, model 3410) were used to deliver pressure into the device through a single inlet (Fig. 1B). In-house electronics and control scripts were constructed to regulate and monitor pressure, and to record the electrical resistance of strain sensors. A fixed voltage of 2.5 V was applied across each CNT strain sensor and the electrical current was measured at a sampling frequency of 10 Hz using a precision ammeter (Keithley sourcemeter model 2602). The sensors were preconditioned using a minimum of 6 h strain runs per day for three days prior to calibration to ensure reproducible strain signals.

During calibration, the bulging height at the center of each membrane was experimentally measured against the actuation pressure applied, using a Navitar zoom system (Navitar, Rochester, NY) and a CCD camera, as shown in Movie S1. A cyclic driving pressure with step-wise decreasing magnitude was applied. The pressure magnitude was decreased from 8 to 2 kPa in 9 equal steps. Correspondingly, the peak-to-peak magnitude of the resistive strain of the CNT sensors decreased from 0.05 to 0.002 also in 9 equal steps and was recorded to correlate with the magnitude of free bulging height of the membrane (without the presence of a sample on top) (Fig. 2A). The relation between the membrane deflection magnitude and the resistive strain magnitude, $|\Delta R/R_0|$ (Fig. 2B), was used to convert the recorded CNT sensor signal on the cultured hydrogel constructs to corresponding membrane deflection magnitude, which was used to derive the effective modulus of the hydrogel construct (Fig. 2C). 3D dynamic mechanical stretching of cell seeded PEG-NB arrays was performed by applying a triangle waveform pressure at 0.1 Hz. The PEG-NB hydrogel array in the device dedicated for 3D mechanical stimulation was statically cultured for one day to allow for swelling to equilibrium and then was cyclically stretched for 14 days while the sensor signal of resistance was continuously recorded. The sensor signal data was obtained from different sensors from at least three experiments.

Supplementary video related to this article can be found at https://doi.org/10.1016/j.biomaterials.2018.04.041.

### 2.5. On-chip tissue stiffness measurement

For a given actuation pressure, membrane deflection was proportional to the sample stiffness and was monitored by the resistive strain magnitude of the CNT sensor, $|\Delta R/R_0|$ (Fig. 2A). The signal $|\Delta R/R_0|$ was then converted to the membrane deflection based on the calibration curve (Fig. 2B). Finally, the membrane deflection magnitude was input into the numerical models (see next section) to calculate the corresponding gel stiffness. In the control group, CNT sensors without bound gels were used to monitor the baseline signal over the culturing period, and were used to compare with the recorded signal from bonded gels to derive the relative signal changes. The $|\Delta R/R_0|$ values measured at different time points were first normalized to their initial values at day 1, then those $|\Delta R/R_0|$ values measured from the gels were further normalized to the average of $|\Delta R/R_0|$ from the control sensors to reveal the relative difference caused by the stiffness changes in the gels.

### 2.6. Finite element analysis

3D finite element simulations of the membrane-gel system were performed using ANSYS Workbench v14.0 (ANSYS, Inc., Canonsburg, PA, USA). The PEG-NB gel and OSTE-PDMS were both modelled as nearly incompressible isotropic elastic material with assumed Poisson's ratio of 0.49. Optical images were experimentally taken and analyzed using ImageJ (NIH) to determine the thickness of the OSTE-PDMS device layer, and dimensions of the PEG-NB gel for modeling in ANSYS. The OSTE-PDMS membrane typically had a thickness of ~1 mm and a gap distance underneath it of 0.3 mm. The portion of the OSTE-PDMS material without the gap was included beyond the gap region to match the physical system (Fig. S1). In the numerical model, the gel was set to be physically bound to the OSTE-PDMS membrane. The tensile modulus of OSTE-PDMS (284 kPa [26]) and elastic modulus of PEG-NB gels as well as the peak pressure applied were inputted to the FEA model, and the strain distribution and membrane deflection was read as the output of the simulation. To estimate the unknown modulus of gels during real-time strain sensing, the forward FEA that predicts the OSTE-PDMS membrane deflection based on the input material parameters was iterated with a sweep of gel moduli to match the numerically predicted membrane deflection with that derived from experimentally measured sensor signals. This process is referred to as inverse FEA hereafter.

### 2.7. Mechanical compression testing

The gel samples from different conditions were taken off and collected from each device at days 1, 7, and 15, and were immediately compression tested before fixation for immunostaining. The compressive moduli of cell-embedded PEG-NB gel samples were characterized from unconfined compression tests using a commercial mechanical test machine (TestResources 840 series). Unconfined compression was performed because it is a standard test configuration that reasonably approximates the loading on the device [26] and has been shown to yield accurate measurements of tensile properties [34]. Briefly, each sample was cyclically compressed to 20% strain while the data of position and applied force were collected. Images of samples were taken and analyzed using ImageJ to measure the cross-section areas and initial heights. The compressive modulus was calculated by fitting the corresponding approaching stress-strain curve from the last cycle.

### 2.8. Immunostaining

To assess the effect of extended 3D mechanical stimulation on cell responses, MSCs embedded in the PEG-NB gels were stained for α-smooth muscle actin (α-SMA), a biomarker of myofibroblasts, and collagen type I (Col I) for collagen production. The neo-expression and incorporation of α-SMA into stress fibers are considered to be the defining characteristic of differentiated myofibroblast [35]. Thus, single cell immunofluorescence-based analysis is appropriate to identify the proportion of functional myofibroblasts in a population of cells. The PEG-NB gels assigned for immunostaining were thrice washed with 1× TBS followed by incubation with 10% neutral buffered formalin fixative for one hour at room temperature (RT). The gels were subsequently washed with TBS and stored at 4 °C prior to staining. To prepare fixed samples for immunostaining, the gels were first permeabilized with TBS containing 0.25% Triton X-100. Following permeabilization, gels were blocked with 10% bovine serum albumin in TBS for one hour at RT. After blocking, gels were incubated with rabbit monoclonal anti-collagen type I primary antibodies (ab138492, Abcam; 1:300 dilution) in TBS containing 5% goat serum (GS) overnight at 4 °C. The next day, gels were washed with TBS four times and blocked with 10% GS in TBS for one hour at RT followed by incubation with Alexa Fluor 568 goat anti-rabbit secondary antibodies (1:300) in TBS containing 5% GS for 1.5 h at RT in the dark. The gels were then washed four times with TBS and incubated with FITC-conjugated mouse monoclonal anti-human α-SMA (F3777, Sigma; 1:300) in TBS with 5% GS overnight at 4 °C. Next, gels were washed four times with TBS and incubated with Hoechst 33342 (P162249, Fisher; 1:50) for 15 min at RT. The gels were washed again, first with TBS then with deionized water. Finally, Fluoromount combined with deionized water were added to cover each gel for signal preservation prior to imaging with confocal microscopy.

### 2.9. Confocal microscopy imaging and analysis

Optical slice images (Z-stack) of stained MSCs were acquired with a laser scanning confocal microscope (Nikon A1R-A1) using a 10× objective (CFI Plan Apo λ 10×/0.45, Nikon). Each PEG-NB gel was imaged at the central region where the nominal tensile strain was calculated (Fig. S1). For imaging cells stained for α-SMA and Col I, the PEG-NB gels were imaged from the top side. Using ImageJ the z-stack images were divided to individual channels of nucleus, α-SMA and Col I. Stacked images in each channel were then projected to a single image. A copy of the single image was automatically thresholded to generate a mask that was applied back to the original single image for measuring different properties of outlined objects in each channel. The averaged area and integrated density of fluorescence intensity of α-SMA and Col I were normalized to those of the nuclei for each stack. Multiple stacks from each gel were averaged for comparison.

### 2.10. Statistical analysis

Statistical analysis was performed using SigmaPlot 12.0. Data are reported as mean ± standard error of the mean (SEM) unless otherwise noted and were analyzed by one-way and two-way ANOVA with Tukey post hoc tests for all pairwise comparisons. The statistical significance in each comparison was evaluated with $p < 0.05$.

## 3. Results and discussion

### 3.1. Simultaneous 3D mechanical stimulation and strain sensing in situ

Fig. 1 demonstrates the actuation of the deformable membrane platform with integrated strain sensors, configured to apply 3D mechanical stretching to arrayed cell-hydrogel constructs. The PEG-NB gels were firmly bound to and elastically deformed by the OSTE-PDMS membrane as demonstrated previously [26]. The cell-seeded PEG-NB gels under both stimulated and static culture conditions remained bound to the OSTE-PDMS after 15 days of culture. The patterned CNT sensors did not perturb the membrane deflection. The membrane deflection was reflected in the embedded strain sensor signal as shown in Fig. 2A and B. This enabled simultaneous 3D mechanical stimulation and on-chip strain measurement. After sensor pre-conditioning, the strain sensor signal remained stable and constant as shown in Fig. 2A.

During calibration, the magnitude of resistive strain signal accurately correlated to the magnitude of membrane deflection ($R^2 = 0.998$) with varying actuation pressure magnitudes as shown in Fig. 2A and B. The platform was first validated with non-degradable PEG-NB gels as shown in Fig. 2C and D. The effective moduli of non-degradable PEG-NB gels calculated from the sensor signal remained relatively constant over five days (Fig. 2C), which was expected since these gels were cell free and non-degradable. The reference moduli measured from standard offline mechanical compression testing were overlaid for comparison, as shown in Fig. 2D. The effective moduli estimated using our microdevice agreed with those from the standard mechanical testing for a variety of gel stiffness (from 10 to 60 kPa, $R^2 = 0.97$). The on-chip strain sensors presented here have a resolution of 0.053% ± 0.04% (mean ± SD, n = 9) in resistive strain, determined by the resolution of electrical resistance change. This corresponds to a resolution of 1.24 ± 0.77 kPa (mean ± SD, $n = 6$) in the calculated effective modulus.

### 3.2. On-chip strain sensing revealed gel stiffness evolution under 3D mechanical stimulation

Figs. S2 and 3A show the time-course changes in normalized resistive strain magnitude $|\Delta R/R_0|$ and corresponding effective modulus of gels, respectively, from both stretching stimulated and static conditions over the culture period of 14 days (after the one day equilibrium culture as described in Methods Section 4). The effective modulus was calculated from the inverse FEA method (Section 6) based on the membrane deflection magnitude derived from the $|\Delta R/R_0|$ signal. The differences in the normalized $|\Delta R/R_0|$ among the three groups (i.e., stimulated gel vs. static gel vs. control sensor) were statistically significant (all pairwise comparisons, $p < 0.001$). During culture, the normalized $|\Delta R/R_0|$ from cell-seeded PEG-NB gels with 3D mechanical stretching increased gradually from 100% at day 2–107 ± 1% at day 6 (Fig. S2 black), which was significantly higher than the normalized $|\Delta R/R_0|$ from control sensors of 100 ± 2% at day 6 ($p < 0.006$). This corresponded to an increase in the membrane deflection magnitude from day 2 to day 6, indicating gel softening with calculated effective modulus decreasing from 9.3 ± 0.4 kPa at day 2–5.43 ± 1.02 kPa at day 6 (Fig. 3A black). However, starting from day 7 the $|\Delta R/R_0|$ signal from stimulated gels gradually trended downward from 106 ± 1% to 103 ± 1% at day 15 (Fig. S2 black), which was close to the control values of 100 ± 2% at day 15 ($p = 0.41$). This corresponded to a decrease in the membrane deflection magnitude, and an increase in the effective modulus from 5.62 ± 0.93 kPa at day 7–7.95 ± 0.73 kPa at day 15 (Fig. 3A).

In contrast, the normalized $|\Delta R/R_0|$ signal from cell-seeded PEG-NB gels in the static culture condition continued to increase significantly from 100% at day 2–108 ± 1% at day 7–117 ± 2% at day 15 (Fig. S2 white), which were significantly higher than the $|\Delta R/R_0|$ signal from the control sensors ($p < 0.005$). This corresponded to continuous gel softening with the effective moduli decreasing from 9.67 ± 0.55 kPa at day 2–5.22 ± 1.12 kPa at day 7 and to 2.81 ± 0.78 kPa at day 15 (Fig. 3A white), resulting in significantly lower modulus than that of the stretching-stimulated gels ($p < 0.05$).

To verify the on-chip measurement of the changing stiffness of cell-hydrogel constructs, standard unconfined compression testing was conducted on isolated gel samples to characterize and compare the stiffness of the conditioned gels at selected time points (day 1, 7 and 15), as shown in Fig. 3B. The effective moduli estimated from the CNT strain sensors and the compressive moduli were reasonably consistent at all time points and for both static and stretched samples, considering the variability between the device and reference moduli (Fig. 2C and D) and the resolution of the device measurements. As measured with the CNT strain sensors, the compressive moduli of the static control gels decreased continuously and significantly from 8.15 ± 0.53 kPa at day 1–3.72 ± 0.60 kPa at day 7 and to 1.21 ± 0.46 kPa at day 15 ($p < 0.05$ for all pairwise comparison, Fig. 3B white). In contrast, the compressive moduli of the stretching stimulated gels first decreased significantly from 8.15 ± 0.53 kPa at day 1–3.16 ± 0.66 kPa at day 7 ($p < 0.005$, Fig. 3B), but then increased significantly after day 7 to 6.36 ± 0.38 kPa at day 15 ($p < 0.005$), which was not significantly different from the original value at day 1 ($p = 0.083$). The difference in the compressive moduli between the static and stimulated conditions at day 7 was insignificant (i.e., 3.72 ± 0.6 vs. 3.16 ± 0.66 kPa, $p = 0.47$), but became apparent and significant at day 15 (i.e., 1.21 ± 0.46 vs. 6.36 ± 0.38 kPa, $p < 0.001$). These comparisons again are consistent with the trends captured by the CNT strain sensor signals and the estimated effective moduli as shown in Figs. 3A and S2, and validate our platform for measuring the stiffness of soft biomaterials in situ over time. Greater lateral and vertical spatial resolution measurement of local construct stiffness and its association with local cell responses could be investigated with alternative spatial arrangements of multiple strain sensors per membrane and more complex material models for the inverse FEA.

By comparing hydrogels with developing stiffness that were either in 3D stretching stimulated or static conditions, we demonstrated that these events can be monitored by in situ stiffness measurement. Here we showed the measurement of elastic moduli of soft biomaterials in the range of $1\ \text{kPa} < E < 60\ \text{kPa}$. For 3D stretching stimulation, we selected 5% nominal tensile strain because it was shown by us and others to promote MSCs and MSC-like cells differentiation to myofibroblasts [26,36]. Application of higher tensile strain levels (up to 40%) can be achieved by applying higher magnitude of driving pressure to our microdevice. The operation of the CNT strain sensors is independent of the selected driving pressure within the calibrated range. While not demonstrated here, this allows for fine tuning of 3D mechanical stimulation in future applications with on-line stiffness measurement. Notably, with the actuation pressure kept constant, an original strain profile designed for the cells would be inevitably altered with gradual changes in gel stiffness due to degradation and remodeling. Thus, the applied mechanical stimulation to cells and the interpretation of biological responses would be confounded by the deviation from the originally prescribed strain, which is often overlooked in literature. This indeed necessitates the capability to closely monitor the changes of applied strain and account for strain deviation for informed analysis.

### 3.3. Mechanical stimulation regulates cell network formation and collagen expression

To characterize cell responses and collagen production, we co-stained the embedded MSCs for α-SMA to probe myofibroblast differentiation and collagen type I as it is the major structural ECM protein in most connective and load-bearing tissues. We confined analysis of the MSCs to those in the central region with relatively homogeneous 5% tensile strain (Fig. S1). While not conducted here, spatial differences in cell responses and their correlation to local strains (Fig. S1) can be investigated by regional imaging, as demonstrated previously [26]. Fig. 4A–E shows the representative confocal fluorescent images of optical slices of cells, reconstructed and projected as maximum intensity projections, at day 1 (Fig. 4A), day 7 (Fig. 4B and C) and day 15 (Fig. 4D and E). Fig. 4A shows the staining of MSCs prior to the application of 3D mechanical stretching, which was used to represent the starting point for both static control and stimulated conditions. Cell shapes at day 1 were mostly spherical with baseline level of α-SMA staining, no stress fibers, and minimal collagen staining (Fig. 4A). Under static culture, a portion of cells were found to be spread at day 7 (arrows in Fig. 4B), as also reflected by a significant increase in the nuclear aspect ratio from 1.64 ± 0.01 at day 1–2.01 ± 0.05 at day 7 ($p < 0.001$, Fig. 4F). Compared to day 1, there was no significant increase in α-SMA expression ($p > 0.13$, Fig. 4G) but a significant increase in collagen expression in normalized average area of collagen staining per cell from 1.62 ± 0.47 at day 1–4.13 ± 0.66 at day 7 ($p = 0.014$, Fig. 4H). The gel geometry remained largely unchanged compared to day 1 (Fig. 4B bright field image) although the gels were significantly softened as shown in Fig. 3. In comparison, static gels by day 15 were noticeably degraded, especially in the central region resulting in a valley, likely due to cell-driven gel

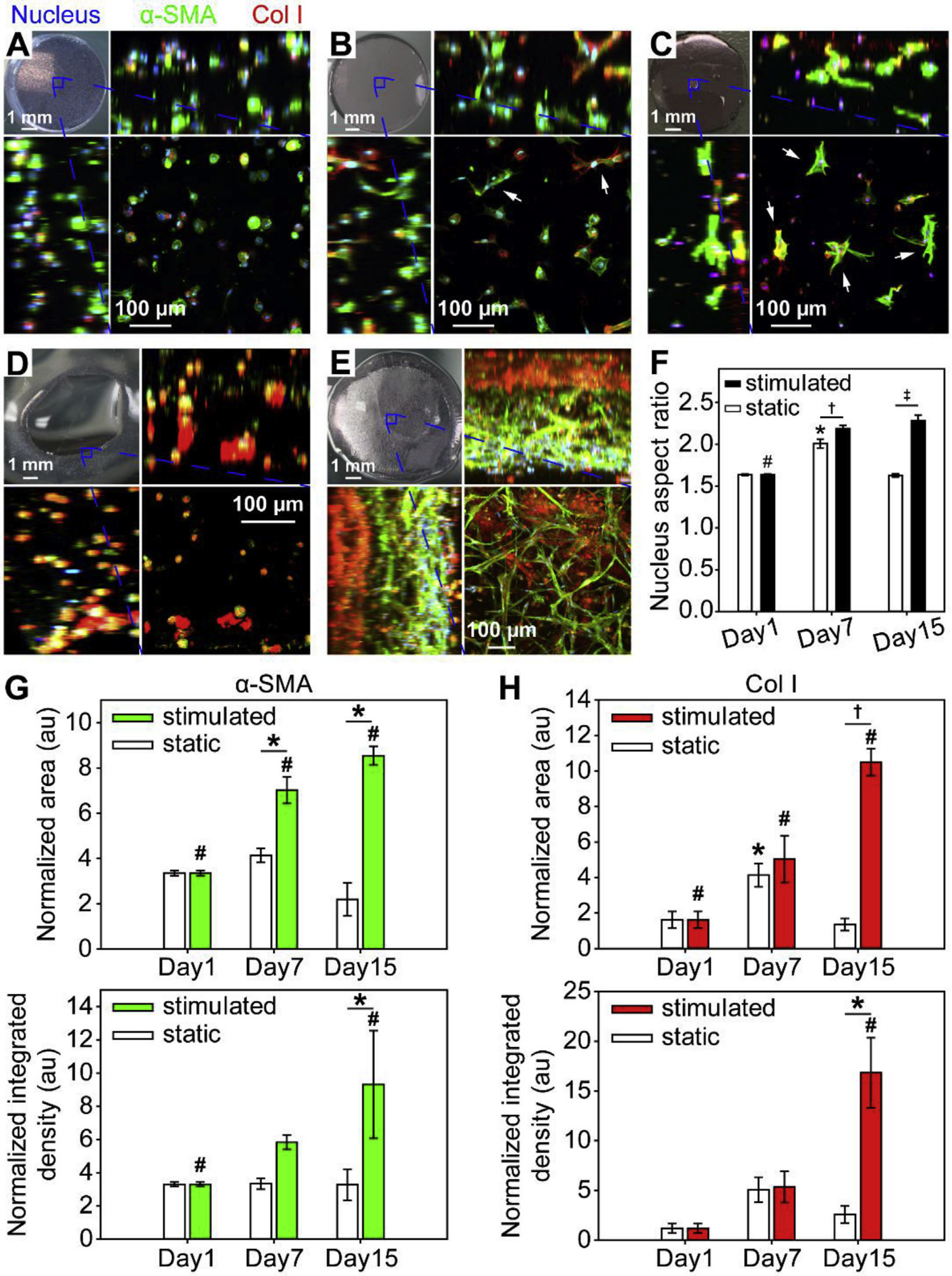

**Fig. 4.** Representative confocal images of immunostaining embedded MSCs in PEG-NB gels under (A) static culture at day 1, (B) static culture at day 7, (C) 3D stretching stimulation at day 7, (D) static culture at day 15 and (E) mechanical stimulation at day 15. Top-left: top-view optical image of the representative gel; left and top: side-view projections. The images were taken at the gel center regions. (F) Nucleus aspect ratios were used to characterize cell elongation (${}^{*}p < 0.001$ vs. other groups in static condition, #$p < 0.001$ vs. other groups in stimulated condition, †$p = 0.004$, ±$p < 0.001$, $n = 3$–6 per group). Quantities of projected area (top) and integrated density of fluorescent intensity (bottom), both normalized to nucleus, were used to characterize cell responses for (G) α-SMA (${}^{*}p < 0.001$, #$p < 0.05$ between groups with symbol) and (H) Col I (top, ${}^{*}p < 0.05$ vs. other groups in static condition, #$p < 0.05$ between groups with symbol, †$p < 0.001$) (bottom, ${}^{*}p < 0.001$, #$p < 0.001$ vs. other groups in stimulated condition). $n = 3$–6 per group; error bars indicate s.e.m.

degradation [37,38], although other factors may have contributed. An indirect measure of gel degradation is to assess cell morphology, as the cells were initially rounded and confined when encapsulated in the covalently crosslinked gels (Fig. 4). Since the gels were crosslinked by peptides that are MMP cleavable, the gels would be readily de-crosslinked as the embedded cells started to proliferate, spread and migrate with increased MMP activity [39]. By day 15, the static gels were so significantly degraded that they were unable to maintain the cylindrical geometry (Fig. 4D bright field image), corresponding with the significant decrease in gel stiffness as shown in Fig. 3, and the embedded cells mostly became spherical in shape by day 15 (Fig. 4D fluorescent images). This was also indicated by the significant decrease in the nuclear aspect ratio from 2.01 ± 0.05 at day 7 to 1.63 ± 0.02 at day 15 ($p < 0.001$, Fig. 4F) close to the initial levels of 1.64 ± 0.01 at day 1, likely due to loss of adhesion to the degraded gels. The normalized area of collagen per cell also significantly decreased from 4.13 ± 0.66 at day 7 to 1.35 ± 0.34 at day 15 ($p = 0.027$, Fig. 4H).

Similar to the static culture condition, gels that were stretched softened at day 7 (as shown in Fig. 3) but their cylindrical geometry remained unchanged compared to day 1 (Fig. 4C bright field image). However, cells in stimulated gels were more spread at day 7 compared to the static culture (arrows in Fig. 4C). This was reflected by a significant increase between static and stimulated conditions in the nuclear aspect ratio from 2.01 ± 0.05 to 2.19 ± 0.04 ($p = 0.004$, Fig. 4F), as well as an increase in the normalized average area of α-SMA staining per cell from 4.14 ± 0.31 to 7.03 ± 0.58 ($p < 0.001$, Fig. 4G). Stretch-stimulated cells generated a significant but similar increase to the static culture in the normalized area of collagen from 1.62 ± 0.47 at day 1–5.04 ± 1.32 at day 7 ($p = 0.006$, Fig. 4H). By day 15, stretching stimulated gels were swollen in size likely also due to cell-mediated gel degradation, but in contrast to the static culture condition, the integrity of the stimulated gels was maintained and the cylindrical geometry was conserved (Fig. 4E bright field image). Interestingly, networks composed of bundles of elongated cells formed throughout the gels (Fig. 4E, S3 and S4). Differences in cell elongation in the gels were evident in the differences in nuclear aspect ratio between stimulated (2.28 ± 0.06) and static (1.63 ± 0.02) conditions ($p < 0.001$, Fig. 4F). The expression of α-SMA (measured by normalized area) was significantly increased during the culture from 3.35 ± 0.11 at day 1–7.03 ± 0.58 at day 7–8.54 ± 0.41 at day 15 ($p < 0.05$ for each comparison between any two days, Fig. 4G top). Compared to the static culture at day 15, stretching stimulation also resulted in significantly higher normalized area of α-SMA of 8.54 ± 0.41 vs. 2.19 ± 0.73 from static condition ($p < 0.001$, Fig. 4G top), and higher integrated density of α-SMA of 9.31 ± 3.24 vs. 3.28 ± 0.93 from static condition ($p < 0.001$, Fig. 4G bot). In addition, substantial collagen was produced at the top region of the gels during culture with stretching stimulation (Fig. 4E, S3 and S4), which resulted in the significant increase in the normalized area of collagen from 5.04 ± 1.32 at day 7–10.5 ± 0.76 at day 15 ($p < 0.001$, Fig. 4H top), as well as in the integrated density of collagen from 5.36 ± 1.56 at day 7–16.84 ± 3.51 at day 15 ($p < 0.001$, Fig. 4H bot). Compared to the static culture at day 15, the significant collagen production with stretching stimulation resulted in more than six-fold increase in both normalized area and integrated density of collagen ($p < 0.001$, Fig. 4H). The responses of MSCs to stretch observed in this study were qualitatively similar to those observed in a similar platform but without embedded CNT strain sensors [26], implying that the cells were not influenced by the presence of the CNT sensors.

The formation of an entangled and α-SMA-rich cell network and significant production of collagen at day 15 resulting from the application of 3D stretching stimulation contributed to maintaining the integrity of gels and tissue growth and led to the significant recovery of hydrogel stiffness after the initial degradation-caused gel softening as measured in Fig. 3. The prevalence of cell network was attributable to a combined effect of increased number of cells and spreading/elongation (Fig. 4, S3 and S4) that are likely enhanced by mechanical stimulation [36,40,41]. 3D mechanical stimulation has been shown to greatly affect MSC activities such as proliferation, migration and differentiation [14,42–44]. In particular, many cell types increase collagen synthesis in response to mechanical stimuli [45,46]. In contrast, the culturing of cells under static conditions resulted in continuous degradation of the gels that correlated with significant and monotonic decrease of hydrogel stiffness (Fig. 3). This is likely attributable to the mismatch in cell-mediated gel degradation and structural reinforcement by ECM production and/or cell network formation during culture. This emphasizes the importance of achieving a balanced cell driven matrix degradation and remodeling during tissue development [47,48], as well as the importance of 3D mechanical stimulation in promoting MSC myofibrogenesis and collagen production.

Similar to our previous report [26], significantly higher expression in α-SMA was observed from stretching stimulated conditions in comparison to the static culture by day 7. In contrast, the difference in collagen expression at day 7 was indistinguishable, suggesting that stretching stimulated matrix protein expression lagged α-SMA expression (Fig. 4) [39]. Interestingly, by day 15 there was a discrepancy between locations with significant α-SMA and collagen expression with 3D stretching stimulation (Fig. 4E). Compared to the cells highly expressing α-SMA indicative of contractile myofibroblastic differentiation (with stress fibers formation as shown in Fig. S5), collagen was produced more significantly on the top/surface of the gels. The reasons for the spatial heterogeneity in collagen production are unclear. Ku et al. reported that MSCs and MSC-like cells rapidly (i.e., within a week) secreted collagen isoforms in response to physiological levels of mechanical stretching in 2D [49]. It is indeed suggested that the upregulation of matrix remodeling by MSC-like cells depends on dimensionality (i.e., 2D > 3D) [50], which possibly contributed to the observed discrepancy in collagen production between gel top surface and lower parts. In addition, the diffusion gradient of the supplemented ascorbic acid, necessary for collagen formation, may also be a factor [51]. Myofibroblast differentiation of MSC-like cells can be induced and observed within a few days of culture in both 2D and 3D conditions in vitro [15,52], but extensive collagen production in 3D is expected to take longer (e.g., >3 weeks) [39].

### 3.4. *Measurement of compressive stiffness of hydrogel constructs in situ*

To demonstrate the versatility of the platform, we also operated the device array to monitor in-situ the compressive stiffness of MSC-laden PEG-NB gels cultured under osteogenic conditions without mechanical stimulation (method details described in the Supporting Information). As shown in Fig. 5A and B, by confining samples in the chamber, mechanical compression can be applied to the samples via bulging the membranes from underneath. To minimize the stimulatory effects of compressive mechanical loading on cells during measurement, we limited measurement cycles to 20–30 min applied every two to three days. As shown in Fig. 5C, PEG-NB gels with seeded cells had similar stiffness of 15.85 ± 3.47 kPa at day 3 compared to 15.19 ± 2.98 kPa at day 1, but then significantly stiffened to 48.41 ± 7.39 kPa at day 7, 62.5 ± 8.56 kPa at day 11, and 64.87 ± 8.17 kPa at day 21 ($p < 0.002$ vs. day 1). The day 21 stiffness is comparable to compressive moduli (e.g. 59 kPa) reported by others for cell-seeded PEG gels cultured for 21 days under osteogenic conditions [53,54]. Significant stiffening correlated with mineralization throughout the hydrogel interior and in a ~20 μm thick cell layer that formed on the exterior of hydrogel (Fig. 5D and E; Fig. S6). Although not demonstrated here, this platform would enable the investigations of the effect of extended 3D compressive mechanical stimulation on MSC osteogenesis with continuous measurements of compressive stiffness.

## 4. Conclusion

This paper reported a new deformable membrane platform with integrated CNT strain sensors that enables simultaneous

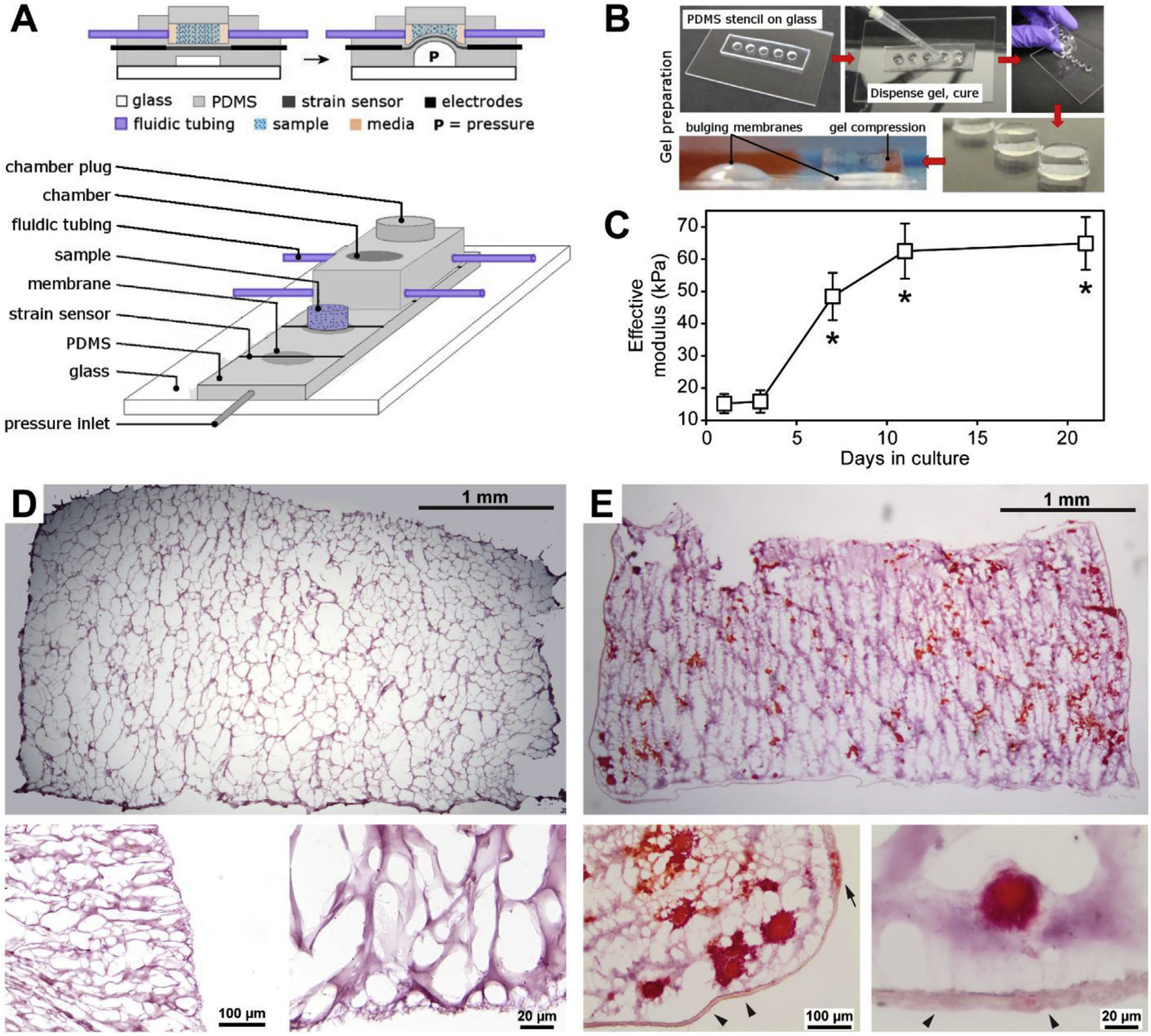

**Fig. 5.** Deformable membrane platform with on-chip strain sensors in compression mode of operation. (A) Samples are confined between flat solid chamber plugs at the top and deformable membranes at the bottom that are deflected by driving pressure. CNT-based strain sensors provide continuous readout of membrane deflection magnitude. Independent chambers are perfused separately. (B) Cell-laden PEG-NB hydrogels were photopolymerized, cast in a PDMS stencil and loaded into chambers as demonstrated. (C) Measured cell-PEG-NB construct compressive modulus during 21 days of culture. Cells were seeded at $2.5 \times 10^5$ cells/mL with osteogenic culture medium. Gel stiffness increased over time and reached similarly high values after 11 days in culture. $^*p < 0.002$ compared to day 1. All data are mean ± SEM, n = 4. (D–E) Alizarin Red staining of calcium deposits in cell-PEG-NB constructs cultured for 1 day (D) and 21 days (E) in osteogenic media. Arrow heads indicate cell-dense sheath encapsulating the gel; arrow indicates mineralized nodules in the cell sheath.

mechanical stimulation of 3D cell-hydrogel arrays and stiffness measurement of the hydrogel constructs in situ. Significant evolution in the stiffness of the cell-hydrogel constructs during culture was detected by the on-chip strain sensors and correlated with tissue production and hydrogel degradation observed (immuno) histomorphmetrically. This platform offers a unique approach to continuously monitor the functional stiffness of cultured tissue constructs in situ instead of relying on end-point analysis. This measurement technique could be transferred and generalized to other relevant organ-on-a-chip platforms to facilitate the establishment of on-line, non-invasive, and high-throughput functional analysis as required to realize the full potential of organ-on-a-chip technologies. The platform also enables future exploration of bioprocess control strategies for in vitro tissue maturation and can provide insights into the dynamics of engineered tissue development that are otherwise not readily available.

## Data availability

The raw/processed data required to reproduce these findings cannot be shared at this time as the data also forms part of an ongoing study.

## Acknowledgements

We thank Oleg Chebotarev for his assistance with platform electronics and software development. We thank Andrea Kwong and Mark Blaser for their assistance with histological sample preparation. The authors acknowledge financial support from Canadian Institute of Health Research (CIHR) Operating Grant (MOP-130481), the Canada Research Chair in Mechanobiology to CAS and Micro and Nanoengineering Systems to YS and NSERC CREATE Program in Microfluidic Applications and Training in Cardiovascular Health (MATCH) scholarship, and Heart and Stroke Richard

Lewar Centre of Excellence (HSRLCE) studentship to HL.

## Appendix A. Supplementary data

Supplementary data related to this article can be found at https://doi.org/10.1016/j.biomaterials.2018.04.041.

## References

[1] B.M. Baker, C.S. Chen, Deconstructing the third dimension: how 3D culture microenvironments alter cellular cues, J. Cell Sci. 125 (2012) 3015–3024, https://doi.org/10.1242/jcs.079509.

[2] P.W. Riem Vis, J. Kluin, J.P.G. Sluijter, L.A. van Herwerden, C.V.C. Bouten, Environmental regulation of valvulogenesis: implications for tissue engineering, Eur. J. Cardio. Thorac. Surg. 39 (2011) 8–17, https://doi.org/10.1016/j.ejcts.2010.05.032.

[3] J. Usprech, W.L.K. Chen, C.A. Simmons, Heart valve regeneration: the need for systems approaches, Wiley Interdiscip. Rev. Syst. Biol. Med 8 (2016) 169–182, https://doi.org/10.1002/wsbm.1329.

[4] P.J. Hung, P.J. Lee, P. Sabounchi, R. Lin, L.P. Lee, Continuous perfusion microfluidic cell culture array for high-throughput cell-based assays, Biotechnol. Bioeng. 89 (2005) 1–8, https://doi.org/10.1002/bit.20289.

[5] J.A. Burdick, G. Vunjak-novakovic, Engineered microenvironments for controlled stem cell differentiation, Tissue Eng. 15 (2009), https://doi.org/10.1089/ten.tea.2008.0131.

[6] E. Figallo, C. Cannizzaro, S. Gerecht, J.A. Burdick, R. Langer, N. Elvassore, G. Vunjak-Novakovic, Micro-bioreactor array for controlling cellular microenvironments, Lab Chip 7 (2007) 710–719, https://doi.org/10.1039/b700063d.

[7] D.M. Titmarsh, J.E. Hudson, A. Hidalgo, A.G. Elefanty, E.G. Stanley, E.J. Wolvetang, J.J. Cooper-White, Microbioreactor arrays for full factorial screening of exogenous and paracrine factors in human embryonic stem cell differentiation, PLoS One 7 (2012), https://doi.org/10.1371/journal.pone.0052405.

[8] S. Gobaa, S. Hoehnel, M. Roccio, A. Negro, S. Kobel, M.P. Lutolf, Artificial niche microarrays for probing single stem cell fate in high throughput, Nat. Methods 8 (2011) 949–955, https://doi.org/10.1038/nmeth.1732.

[9] A. Peters, D.M. Brey, J.A. Burdick, High-throughput and combinatorial technologies for tissue engineering applications, Tissue Eng. Part B Rev. 15 (2009) 225–239, https://doi.org/10.1089/ten.teb.2009.0049.

[10] J. Usprech, D.A. Romero, C.H. Amon, C.A. Simmons, Combinatorial screening of 3D biomaterial properties that promote myofibrogenesis for mesenchymal stromal cell-based heart valve tissue engineering, Acta Biomater. 58 (2017) 34–43, https://doi.org/10.1016/j.actbio.2017.05.044.

[11] N. Tandon, D. Marolt, E. Cimetta, G. Vunjak-Novakovic, Bioreactor engineering of stem cell environments, Biotechnol. Adv. 31 (2013) 1020–1031, https://doi.org/10.1016/j.biotechadv.2013.03.007.

[12] D.E. Jaalouk, J. Lammerding, Mechanotransduction gone awry, Nat. Rev. Mol. Cell Biol. 10 (2009) 63–73, https://doi.org/10.1038/nrm2597.

[13] P.R. LeDuc, W.C. Messner, J.P. Wikswo, How do control-based approaches enter into biology? Annu. Rev. Biomed. Eng. 13 (2011) 369–396, https://doi.org/10.1146/annurev-bioeng-071910-124651.

[14] L. MacQueen, Y. Sun, C.A. Simmons, Mesenchymal stem cell mechanobiology and emerging experimental platforms, J. R. Soc. Interface 10 (2013), https://doi.org/10.1098/rsif.2013.0179, 20130179–20130179.

[15] C. Moraes, M. Likhitpanichkul, C.J. Lam, B.M. Beca, Y. Sun, C.A. Simmons, Microdevice array-based identification of distinct mechanobiological response profiles in layer-specific valve interstitial cells, Integr. Biol. (Camb) 5 (2013) 673–680, https://doi.org/10.1039/c3ib20254b.

[16] Y. Kamotani, T. Bersano-Begey, N. Kato, Y.-C. Tung, D. Huh, J.W. Song, S. Takayama, Individually programmable cell stretching microwell arrays actuated by a Braille display, Biomaterials 29 (2008) 2646–2655, https://doi.org/10.1016/j.biomaterials.2008.02.019.

[17] A. Khademhosseini, R. Langer, J. Borenstein, P.J. Vacanti, Microscale technologies for tissue engineering and biology, Proc. Natl. Acad. Sci. 103 (2006) 2480–2487, https://doi.org/10.1073/pnas.0507681102.

[18] F. Rehfeldt, A.J. Engler, A. Eckhardt, F. Ahmed, D.E. Discher, Cell responses to the mechanochemical microenvironment-Implications for regenerative medicine and drug delivery, Adv. Drug Deliv. Rev. 59 (2007) 1329–1339, https://doi.org/10.1016/j.addr.2007.08.007.

[19] C.C. DuFort, M.J. Paszek, V.M. Weaver, Balancing forces: architectural control of mechanotransduction, Nat. Rev. Mol. Cell Biol. 12 (2011) 308–319, https://doi.org/10.1038/nrm3112.

[20] D.-L. Wang, S.-D. Jiang, L.-Y. Dai, Biologic response of the intervertebral disc to static and dynamic compression in vitro, Spine (Phila. Pa. 1976) 32 (2007) 2521–2528, https://doi.org/10.1097/BRS.0b013e318158cb61.

[21] E.A. Makris, A.H. Gomoll, K.N. Malizos, J.C. Hu, K.A. Athanasiou, Repair and tissue engineering techniques for articular cartilage, Nat. Rev. Rheumatol. 11 (2014) 21–34, https://doi.org/10.1038/nrrheum.2014.157.

[22] W.-H. Zimmermann, Tissue engineering of a differentiated cardiac muscle construct, Circ. Res. 90 (2002) 223–230, https://doi.org/10.1161/hh0202.103644.

[23] Z.H. Syedain, J.S. Weinberg, R.T. Tranquillo, Cyclic distension of fibrin-based tissue constructs: evidence of adaptation during growth of engineered connective tissue, Proc. Natl. Acad. Sci. U. S. A. 105 (2008) 6537–6542, https://doi.org/10.1073/pnas.0711217105.

[24] L. MacQueen, O. Chebotarev, C.A. Simmons, Y. Sun, Miniaturized platform with on-chip strain sensors for compression testing of arrayed materials, Lab Chip 12 (2012) 4178–4184, https://doi.org/10.1039/c2lc40670e.

[25] C. Moraes, G. Wang, Y. Sun, C.A. Simmons, A microfabricated platform for high-throughput unconfined compression of micropatterned biomaterial arrays, Biomaterials 31 (2010) 577–584, https://doi.org/10.1016/j.biomaterials.2009.09.068.

[26] H. Liu, J. Usprech, Y. Sun, C.A. Simmons, A microfabricated platform with hydrogel arrays for 3D mechanical stimulation of cells, Acta Biomater. 34 (2016) 113–124, https://doi.org/10.1016/j.actbio.2015.11.054.

[27] N. Thavandiran, N. Dubois, A. Mikryukov, S. Masse, B. Beca, C.A. Simmons, V.S. Deshpande, J.P. McGarry, C.S. Chen, K. Nanthakumar, G.M. Keller, M. Radisic, P.W. Zandstra, Design and formulation of functional pluripotent stem cell-derived cardiac microtissues, Proc. Natl. Acad. Sci. 110 (2013) E4698–E4707, https://doi.org/10.1073/pnas.1311120110.

[28] M.R. Ebrahimkhani, J.A.S. Neiman, M.S.B. Raredon, D.J. Hughes, L.G. Griffith, Bioreactor technologies to support liver function in vitro, Adv. Drug Deliv. Rev. 69–70 (2014) 132–157, https://doi.org/10.1016/j.addr.2014.02.011.

[29] D. Barata, C. Van Blitterswijk, P. Habibovic, High-throughput screening approaches and combinatorial development of biomaterials using microfluidics, Acta Biomater. 34 (2016) 1–20, https://doi.org/10.1016/j.actbio.2015.09.009.

[30] J.U. Lind, T.A. Busbee, A.D. Valentine, F.S. Pasqualini, H. Yuan, M. Yadid, S. Park, A. Kotikian, A.P. Nesmith, P.H. Campbell, J.J. Vlassak, J.A. Lewis, K.K. Parker, Instrumented cardiac microphysiological devices via multimaterial three-dimensional printing, Nat. Mater. 16 (2016) 303–308, https://doi.org/10.1038/nmat4782.

[31] M.J. Powers, K. Domansky, M.R. Kaazempur-Mofrad, A. Kalezi, A. Capitano, A. Upadhyaya, P. Kurzawski, K.E. Wack, D.B. Stolz, R. Kamm, L.G. Griffith, A microfabricated array bioreactor for perfused 3D liver culture, Biotechnol. Bioeng. 78 (2002) 257–269, https://doi.org/10.1002/bit.10143.

[32] Y. Wen, X. Zhang, S.T. Yang, Microplate-reader compatible perfusion microbioreactor array for modular tissue culture and cytotoxicity assays, Biotechnol. Prog. 26 (2010) 1135–1144, https://doi.org/10.1002/btpr.423.

[33] K. Domansky, W. Inman, J. Serdy, A. Dash, M.H.M. Lim, L.G. Griffith, Perfused multiwell plate for 3D liver tissue engineering, Lab Chip 10 (2010) 51–58, https://doi.org/10.1039/b913221j.

[34] J.G. Williams, C. Gamonpilas, Using the simple compression test to determine Young's modulus, Poisson's ratio and the Coulomb friction coefficient, Int. J. Solid Struct. 45 (2008) 4448–4459, https://doi.org/10.1016/j.ijsolstr.2008.03.023.

[35] J.J. Tomasek, G. Gabbiani, B. Hinz, C. Chaponnier, R.A. Brown, Myofibroblasts and mechano-regulation of connective tissue remodelling, Nat. Rev. Mol. Cell Biol. 3 (2002) 349–363, https://doi.org/10.1038/nrm809.

[36] Y. Cui, F.M. Hameed, B. Yang, K. Lee, C.Q. Pan, S. Park, M. Sheetz, Cyclic stretching of soft substrates induces spreading and growth, Nat. Commun. 6 (2015) 6333, https://doi.org/10.1038/ncomms7333.

[37] E.H. Nguyen, M.R. Zanotelli, M.P. Schwartz, W.L. Murphy, Differential effects of cell adhesion, modulus and VEGFR-2 inhibition on capillary network formation in synthetic hydrogel arrays, Biomaterials 35 (2014) 2149–2161, https://doi.org/10.1016/j.biomaterials.2013.11.054.

[38] K.M. Schultz, K.A. Kyburz, K.S. Anseth, Measuring dynamic cell–material interactions and remodeling during 3D human mesenchymal stem cell migration in hydrogels, Proc. Natl. Acad. Sci. (2015), 201511304, https://doi.org/10.1073/pnas.1511304112.

[39] S.T. Gould, K.S. Anseth, Role of cell-matrix interactions on VIC phenotype and tissue deposition in 3D PEG hydrogels, J. Tissue Eng. Regen. Med. (2013), https://doi.org/10.1002/term.1836.

[40] D.-H. Kim, P.K. Wong, J. Park, A. Levchenko, Y. Sun, Microengineered platforms for cell mechanobiology, Annu. Rev. Biomed. Eng. 11 (2009) 203–233, https://doi.org/10.1146/annurev-bioeng-061008-124915.

[41] G.S. Ugolini, M. Rasponi, A. Pavesi, R. Santoro, R. Kamm, G.B. Fiore, M. Pesce, M. Soncini, On-chip assessment of human primary cardiac fibroblasts proliferative responses to uniaxial cyclic mechanical strain, Biotechnol. Bioeng. 113 (2016) 859–869, https://doi.org/10.1002/bit.25847.

[42] T.M. Maul, D.W. Chew, A. Nieponice, D.A. Vorp, Mechanical stimuli differentially control stem cell behavior: morphology, proliferation, and differentiation, Biomech. Model. Mechanobiol. 10 (2011) 939–953, https://doi.org/10.1007/s10237-010-0285-8.

[43] R.M. Delaine-Smith, G.C. Reilly, Mesenchymal stem cell responses to mechanical stimuli, Muscles. Ligaments Tendons J. 2 (2012) 169–180.

[44] I.L. Ivanovska, J.-W. Shin, J. Swift, D.E. Discher, Stem cell mechanobiology: diverse lessons from bone marrow, Trends Cell Biol. (2015) 1–10, https://doi.org/10.1016/j.tcb.2015.04.003.

[45] Q. Li, Y. Muragaki, I. Hatamura, H. Ueno, A. Ooshima, Stretch-induced collagen synthesis in cultured smooth muscle cells from rabbit aortic media and a possible involvement of angiotensin II and transforming growth factor-beta, J. Vasc. Res. 35 (1998) 93–103, https://doi.org/10.1159/000025570.

[46] M. Ivarsson, A. McWhirter, T.K. Borg, K. Rubin, Type I collagen synthesis in cultured human fibroblasts: regulation by cell spreading, platelet-derived growth factor and interactions with collagen fibers, Matrix Biol. 16 (1998) 409–425.

[47] D. Hanjaya-Putra, K.T. Wong, K. Hirotsu, S. Khetan, J.A. Burdick, S. Gerecht,

Spatial control of cell-mediated degradation to regulate vasculogenesis and angiogenesis in hyaluronan hydrogels, Biomaterials 33 (2012) 6123–6131, https://doi.org/10.1016/j.biomaterials.2012.05.027.

[48] Y. Li, J. Rodrigues, H. Tomás, Injectable and biodegradable hydrogels: gelation, biodegradation and biomedical applications, Chem. Soc. Rev. 41 (2012) 2193–2221, https://doi.org/10.1039/C1CS15203C.

[49] C.-H. Ku, P.H. Johnson, P. Batten, P. Sarathchandra, R.C. Chambers, P.M. Taylor, M.H. Yacoub, A.H. Chester, Collagen synthesis by mesenchymal stem cells and aortic valve interstitial cells in response to mechanical stretch, Cardiovasc. Res. 71 (2006) 548–556, https://doi.org/10.1016/j.cardiores.2006.03.022.

[50] K.M. Mabry, S.Z. Payne, K.S. Anseth, Microarray analyses to quantify advantages of 2D and 3D hydrogel culture systems in maintaining the native valvular interstitial cell phenotype, Biomaterials 74 (2016) 31–41, https://doi.org/10.1016/j.biomaterials.2015.09.035.

[51] C. Vater, P. Kasten, M. Stiehler, Culture media for the differentiation of mesenchymal stromal cells, Acta Biomater. 7 (2011) 463–477, https://doi.org/10.1016/j.actbio.2010.07.037.

[52] W. Kim, D.A. Barron, R. San Martin, K.S. Chan, L.L. Tran, F. Yang, S.J. Ressler, D.R. Rowley, RUNX1 is essential for mesenchymal stem cell proliferation and myofibroblast differentiation, Proc. Natl. Acad. Sci. 111 (2014) 16389–16394, https://doi.org/10.1073/pnas.1407097111.

[53] S.H. Parekh, K. Chatterjee, S. Lin-Gibson, N.M. Moore, M.T. Cicerone, M.F. Young, C.G. Simon, Modulus-driven differentiation of marrow stromal cells in 3D scaffolds that is independent of myosin-based cytoskeletal tension, Biomaterials 32 (2011) 2256–2264, https://doi.org/10.1016/j.biomaterials.2010.11.065.

[54] K. Chatterjee, S. Lin-Gibson, W.E. Wallace, S.H. Parekh, Y.J. Lee, M.T. Cicerone, M.F. Young, C.G. Simon, The effect of 3D hydrogel scaffold modulus on osteoblast differentiation and mineralization revealed by combinatorial screening, Biomaterials 31 (2010) 5051–5062, https://doi.org/10.1016/j.biomaterials.2010.03.024.